www.sphinxsai.com

International Journal of ChemTech Research
CODEN(USA): IJCRGG ISSN : 0974-4290
Vol.5, No.5, pp 2563.-2574, July-Sept 2013

Experimental And Theoretical Investigation And NBO Analysis On The Structure Of Efavirenz HIV Drug

G.R.Ramkumaar[1]*, T.J.Bhoopathy[1], S.Gunasekaran[1], C. Gokilan[1], S.Srinivasan[2], and Julie Charles[3]

[1]PG and Research Department of Physics, Pachaiyappa's College, Chennai 600030, TN, India
[2]PG and Research Department of Physics, Presidency College, Chennai 600005, TN, India
[3]SSN College of Engineering, Kalavakkam – 603110, kanchipuram District, TN, India.

***Corres.author: gr.ramkumaar@yahoo.com**
Tel.: +91 9884351008

Abstract: A systematic vibrational spectroscopic assignment and analysis of efavirenz has been carried out by using FTIR, FT-Raman and UV spectral data. The vibrational analysis were aided by electronic structure calculations – ab initio (RHF) and hybrid Density Functional methods (B3LYP) performed with 6-31G(d,p) and 6-31++G(d,p) basis sets. Molecular equilibrium geometries, electronic energies, bond orders, natural bond order analysis, IR intensities, and harmonic vibrational frequencies have been computed. The assignments proposed based on the experimental IR and Raman spectra have been reviewed and selected assignment of the observed spectra have been proposed. UV–visible spectrum of the compound was also recorded and the electronic properties, such as HOMO and LUMO energies and λ_{max} were determined by time-dependent DFT (TD-DFT) method. The thermodynamic functions of the title molecule were also performed using the RHF and DFT methods.
Keywords : efavirenz ; UV ; vibrational spectra : Restricted HF; DFT.

1. Introduction

Efavirenz belongs to the class of the non-nucleoside reverse transcriptase inhibitors. Efavirenz exerts its action by non-competitive inhibition of the human immunodeficiency virus type 1 (HIV-1) reverse transcriptase. HIV-2 reverse transcriptase and human cellular DNA polymerases are not inhibited by efavirenz [1]. Treatment of patients with efavirenzmonotherapy rapidly selects for resistant isolates of HIV-1 with the mutation at reverse transcriptase amino acid position 103 (lysine to asparagine) being most frequently observed [1, 2]. However, when administered in combination with nucleoside reverse transcriptase inhibitors and protease inhibitors, efavirenz has demonstrated a potent antiviral effect and is therefore an important addition to the currently available armamentarium of antiretroviral drugs [3–6].

In this present work, an attempt has been made to interpret the vibrational spectra of efavirenz by applying ab initio and Density Functional Theory calculations based on Hartree-Fock and Becke3- Lee-Yang-Parr (B3LYP) level using 6-31G(d,p)and 6-31++G(d,p) basis sets. Further, the calculation of electronic excitations, particularly for valence-like transitions and oscillator strength of efavirenz, were calculated employing the all valence electron TD-DFT methods. In addition to these bond orders and atomic charges

calculated at the RHF/6-31G(d,p), RHF/6-31++G(d,p), B3LYP/6-31G(d,p) and B3LYP/6-31++G(d,p) level. Experimentally observed spectral data of the title compound is found to be well comparable with the data obtained by quantum mechanical methods.

2. Experimental details

The solid phase FTIR spectrum was recorded in the region 4000 - 400 cm^{-1} in evacuation mode on Nexus 670 DTGS using KBr pellet technique with 4.0 cm^{-1} resolution. The FT-Raman spectrum was recorded using 1064 nm line of Nd: YAG laser as excitation wavelength in the region 5000-100 cm^{-1} on Bruker IFS 66V spectrometer equipped with FRA 106 Raman module was used as an accessory. The UV-visible spectrum was recorded on a Varian Cary 5E-UV-NIR spectrophotometer.

3. Computational details

To provide complete information regarding the structural characteristics and the fundamental vibrational modes of efavirenzthe restricted Hartree-Fock and DFT-B3LYP correlation functional calculations have been carried out. The calculations of geometrical parameters in the ground state were performed using the Gaussian 03 [7] programs, invoking gradient geometry optimization [8] on Intel core i3/2.93 GHZ processor. The geometry optimization was carried out using the initial geometry generated from standard geometrical parameters at Hartree-Fock level, and DFT-B3LYP methods adopting 6-31G(d,p) and 6-31++G(d,p) basis sets to characterize all stationary points as minima. The optimized structural parameters of the compound efavirenzwere used for harmonic vibrational frequency calculations resulting in IR and Raman frequencies together with IR intensities. In DFT methods, Becke's three parameter exchange-functional (B3) [9, 10] combined with gradient-corrected correlation functional of Lee, Yang and Parr (LYP) [11] by implementing the split-valence polarized 6-31G(d,p) and 6-31++G(d,p) basis sets [12, 13] have been utilized for the computation of molecular structure optimization, vibrational frequencies, thermodynamic properties and energies of the optimized structures.

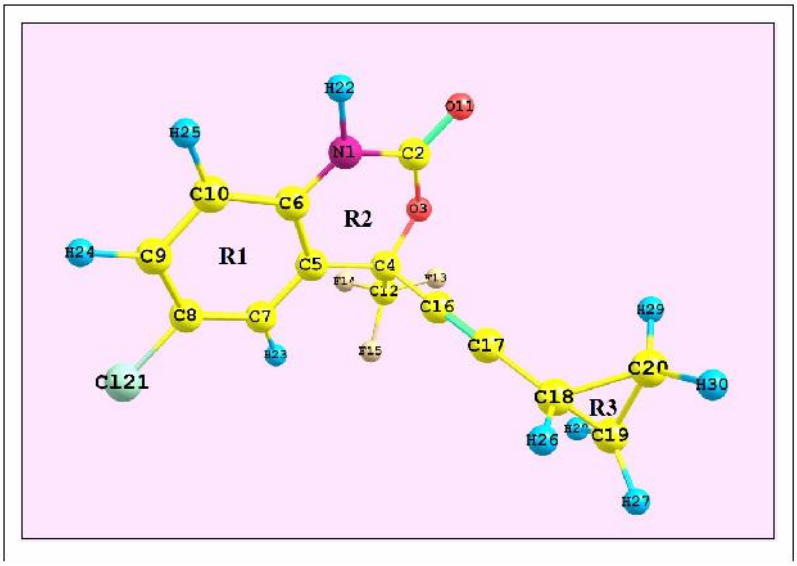

Fig. 1 Atom numbering scheme of efavirenz

Results and Discussion

4.1 Molecular geometry

The molecular structure of efavirenz belongs to C_1 point group symmetry. All vibrations are active in both IR and Raman. The optimized structure parameters of efavirenz calculated by RHF and DFT-B3LYP levels are listed in the Table 1 in accordance with the given Fig. 1 atom numbering scheme of efavirenz. Table 1 compares the calculated bond lengths and angles for efavirenz with those experimentally available data [14]. From the theoretical values, we can find that most of the optimized bond angles are slightly larger than the

experimental values due to the theoretical calculations belonging to isolated molecules in gaseous phase and the experimental results belonging to the molecule in the solid state. Comparing bond angles and bond lengths of B3LYP/6-31G(d,p) and B3LYP/6-31++G(d,p) with those of RHF/6-31G(d,p) and RHF/6-31++G(d,p), as a whole the former are on higher side than the latter. The calculated values correlates well compared to those with the experimental results. In spite of the differences, calculated geometric parameters represent a good approximation and they are the basis for calculating other parameters, such as vibrational frequencies and thermodynamic properties.

Table 1 Structural parameters of efavirenz calculated by RHF and B3LYP methods using 6-31G(d,p) and 6-31++G(d,p) basis sets

Structural parameters	Efavirenz				Ref[14]
	B3LYP/ 6-31G(d,p)	B3LYP/ 6-31++G(d,p)	RHF/ 6-31G(d,p)	RHF/ 6-31++G(d,p)	
Internuclear distance (A˚)					
N1-C2	1.38	1.38	1.36	1.36	1.45
N1-C6	1.40	1.40	1.39	1.39	1.40
N1-H22	1.01	1.01	0.99	0.99	1.01
C2-O3	1.36	1.36	1.34	1.34	1.42
C2-O11	1.21	1.21	1.18	1.18	1.21
O3-C4	1.46	1.46	1.42	1.42	1.43
C4-C5	1.53	1.53	1.53	1.53	1.50
C4-C12	1.55	1.56	1.54	1.54	1.52
C4-C16	1.46	1.46	1.47	1.47	1.47
C5-C6	1.40	1.40	1.39	1.39	1.39
C5-C7	1.39	1.40	1.39	1.39	1.40
C6-C10	1.40	1.40	1.39	1.39	1.40
C7-C8	1.39	1.39	1.38	1.38	1.39
C7-H23	1.08	1.08	1.07	1.07	1.10
C8-C9	1.39	1.40	1.38	1.38	1.39
C8-Cl21	1.76	1.76	1.74	1.74	1.72
C9-C10	1.39	1.39	1.38	1.38	1.40
C9-H24	1.08	1.08	1.07	1.07	1.10
C10-H25	1.09	1.09	1.08	1.08	1.10
C12-F13	1.34	1.34	1.31	1.31	1.39
C12-F14	1.34	1.35	1.32	1.32	1.39
C12-F15	1.35	1.35	1.32	1.32	1.39
F15-H23	2.26	2.28	2.28	2.28	-
C16-C17	1.21	1.21	1.19	1.19	1.21
C17-C18	1.44	1.44	1.45	1.45	1.54
C18-C19	1.52	1.53	1.51	1.51	1.50
C18-C20	1.53	1.53	1.51	1.51	1.50
C18-H26	1.09	1.09	1.08	1.08	1.09
C19-C20	1.50	1.50	1.49	1.49	-
C19-H27	1.09	1.09	1.08	1.08	1.09
C19-H28	1.08	1.08	1.07	1.07	1.09
C20-H29	1.08	1.08	1.07	1.07	1.09
C20-H30	1.09	1.09	1.08	1.08	1.09
Bond angle (◦)					
C2-N1-C6	124.1	124.2	123.7	123.6	114.4
C2-N1-H22	114.1	114.5	114.5	114.7	116.2
C6-N1-H22	119.6	119.7	119.9	119.9	118.2
N1-C2-O3	114.8	114.9	114.7	114.8	114.3
N1-C2-O11	123.8	123.9	123.8	123.8	124.6
O3-C2-O11	121.3	121.1	121.6	121.4	120.3
C2-O3-C4	120.3	120.6	122.0	122.3	121.5
O3-C4-C5	110.3	110.3	110.2	110.3	109.3
O3-C4-C12	101.6	101.2	102.0	101.8	102.3

O3-C4-C16	110.3	110.3	110.3	110.3	111.6
C5-C4-C12	113.3	113.4	113.6	113.6	112.4
C5-C4-C16	110.7	110.8	110.7	110.7	109.3
C12-C4-C16	110.3	110.3	109.8	109.8	109.6
C4-C5-C6	115.5	115.6	115.3	115.4	114.2
C4-C5-C7	124.7	124.7	125.0	124.9	-
C6-C5-C7	119.7	119.6	119.6	119.6	120.2
N1-C6-C5	118.4	118.6	118.5	118.6	-
N1-C6-C10	121.3	121.1	121.1	120.9	120.2
C5-C6-C10	120.3	120.3	120.4	120.4	119.1
C5-C7-C8	119.5	119.6	119.6	119.7	120.1
C5-C7-H23	120.7	120.8	121.0	121.0	119.9
C8-C7-H23	119.8	119.6	119.4	119.3	119.9
C7-C8-C9	121.2	121.1	120.9	120.9	119.9
C7-C8-Cl21	119.3	119.3	119.4	119.4	120.1
C9-C8-Cl21	119.6	119.6	119.7	119.6	120.1
C8-C9-C10	119.3	119.3	119.6	119.5	120.0
C8-C9-H24	120.2	120.3	120.1	120.2	120.0
C10-C9-H24	120.5	120.4	120.3	120.3	120.0
C6-C10-C9	120.1	120.1	119.9	119.9	120.6
C6-C10-H25	119.9	120.0	120.1	120.1	119.7
C9-C10-H25	120.0	120.0	120.1	120.0	119.7
C4-C12-F13	110.9	111.1	110.9	111.0	110.5
C4-C12-F14	111.1	111.3	110.9	111.0	109.5
C4-C12-F15	110.5	110.9	110.9	111.1	110.2
F13-C12-F14	108.6	108.2	108.4	108.2	109.5
F13-C12-F15	107.7	107.4	107.7	107.6	106.3
F14-C12-F15	108.0	107.7	107.9	107.8	107.2
C17-C18-C19	119.9	119.9	119.5	119.5	120.0
C17-C18-C20	119.8	119.8	119.4	119.4	120.0
C17-C18-H26	114.9	114.7	114.2	114.2	-
C19-C18-H26	116.1	116.2	116.9	117.0	-
C20-C18-H26	116.0	116.1	116.9	117.0	-
C18-C19-H27	116.7	116.6	116.9	116.8	115.8
C18-C19-H28	117.0	116.9	117.3	117.3	117.2
C20-C19-H27	118.8	118.8	118.6	118.6	120.0
C20-C19-H28	118.2	118.2	118.2	118.2	-
H27-C19-H28	114.9	115.0	114.8	114.9	113.2
C18-C20-H29	117.0	117.0	117.3	117.2	-
C18-C20-H30	116.7	116.5	116.9	116.8	115.2
C19-C20-H29	118.3	118.2	118.2	118.2	120.0
C19-C20-H30	118.8	118.8	118.6	118.6	118.5
H29-C20-H30	114.9	114.9	114.8	114.9	-

4.2 Bond order analysis

The bond order of efavirenz is presented in Table 2. Bond order is related to bond strength. The bonds with the higher bond order values have short bond length and vice versa. The bond order analysis may predict that the weakest bonds may be cleaved preferentially and they may possess a relatively low pi-bond character. From Table 2, it is noted that bond between C4-C16 possess relatively low pi bond character with low bond order value of 0.79 and 0.80 obtained from RHF and B3LYP method respectively. The C2-O11 bond order values are in the range 1.9, which depict the double bond character, while the C8-Cl21 and C4-C12 bond order value is approximately unity, which shows the single bond character. The strongest bond is C16-C17 with the bond order value of 3.228 and 2.667 predicted from both RHF and B3LYP methods confirms the treble bond character. The optimized geometrical values are in support of the bond order analysis.

Table 2 Bond orders of efavirenz

Bond order	RHF/6-31G(d,p)	B3LYP/6-31G(d,p)
N1-C2	0.966	0.983
N1-C6	0.870	0.893
N1-H22	0.869	0.886
C2-O3	0.876	0.932
C2-O11	1.944	1.981
O3-C4	0.850	0.872
C4-C5	0.989	0.945
C4-C12	1.021	0.940
C4-C16	0.793	0.802
C5-C6	1.419	1.389
C5-C7	1.433	1.424
C6-C10	1.406	1.378
C7-C8	1.417	1.378
C7-H23	0.901	0.891
C8-C9	1.412	1.398
C8-Cl21	1.033	1.014
C9-C10	1.466	1.451
C10-H25	0.952	0.934
C12-F13	0.896	1.005
C12-F14	0.894	1.004
C12-F15	0.843	0.945
C16-C17	3.228	2.667
C17-C18	0.886	1.023
C18-C19	0.942	0.950
C18-C20	0.934	0.947
C18-H26	0.936	0.920
C19-C20	0.942	0.969
C19-H27	0.963	0.948
C19-H28	0.957	0.947
C20-H29	0.964	0.951
C20-H30	0.958	0.944

4.3 Electronic properties

The energies of four important molecular orbitals of efavirenz: the highest and second highest occupied MO's (HOMO and HOMO−1), the lowest and the second lowest unoccupied MO's (LUMO and LUMO+1) were calculated and are presented in Table 3. The lowest singlet→singlet spin-allowed excited states of efavirenz were taken into account for the TD-DFT calculation in order to investigate the properties of electronic absorption. The experimental λ_{max} values are obtained from the UV/visible spectra recorded in methanol. The calculations were also performed with methanol solvent effect. The calculated absorption wavelengths λ_{max}), oscillator strength, excitation energies and the experimental wavelengths are also given in Table 3. The energy gap between HOMO and LUMO is a critical parameter in determining molecular electrical transport properties [15]. In the electronic absorption spectrum of efavirenz, there are three absorption bands with a maximum 298 nm. The strong absorption band 298 nm is caused by the $n \rightarrow \pi^*$ and the other moderately intense bands are due to $\pi \rightarrow \pi^*$ transitions. The $\pi \rightarrow \pi^*$ transitions are expected to occur relatively at lower wavelength, due to the consequence of the extended aromaticity of the benzene ring. The HOMO and LUMO of efavirenz are represented in Fig. 2.

Table 3 Experimental and calculated absorption wavelenght(λ), excitation energies(E), oscillator strength(f) and frontier orbital energies of efavirenz by TD-DFT method

λ(Expt.;nm)	λ(Cal.;nm)	E(eV)	f	Assignment	E_{HOMO}(eV)	E_{LUMO} (eV)	E_{HOMO-1} (eV)	E_{LUMO+1} (eV)
298	304.4	4.6876	0.0359	$n \rightarrow \pi^*$				
248	264.5	4.6876	0.0455	$\pi \rightarrow \pi^{-*}$	-6.0666	-1.1840	-6.9607	-0.6297
	242.8	5.1074	0.1230	$\pi \rightarrow \pi^*$				

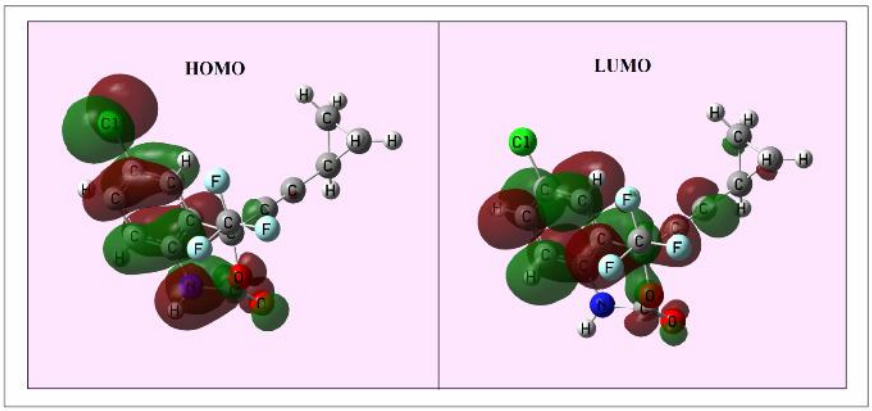

Fig. 2 The HOMO and LUMO of efavirenz

4.4 Natural population analysis

The calculation of effective atomic charges plays an important role in the application of quantum mechanical calculations to molecular systems. My interest here is in the comparison of different methods (RHF/6-31, RHF/6-31++, DFT-B3LYP/6-31 and DFT-B3LYP/6-31++) to describe the electron distribution in efavirenz as broadly as possible, and to assess the sensitivity of the calculated charges to changes in the choice of the quantum chemical method. The calculated natural atomic charge values from the natural population analysis (NPA) and Mulliken population analysis (MPA) procedures using the RHF/6-31, RHF/6-31++, DFT-B3LYP/6-31 and DFT-B3LYP/6-31++ methods are listed in Table 4. The NPA from the natural bonding orbital (NBO) method is better than the MPA scheme. Table 4 compares the atomic charge site of efavirenz from both MPA and NPA methods. The NPA of efavirenz shows that the presence of two oxygen atoms [O3 = -0.635 (RHF/6-31), -0.632(RHF/6-31++), -0.560(DFT-B3LYP/6-31) and -0.553(DFT-B3LYP/6-31++); O11= -0.619(RHF/6-31), -0.614(HF/6-31++), -0.516(DFT-B3LYP/6-31), and -0.516(DFT-B3LYP/6-31++)] imposes large positive charges on the carbon atom [C2 = 1.142 (RHF/6-31), 1.127(RHF/6-31++), 0.961(DFT-B3LYP/6-31) and 0.947(DFT-B3LYP/6-31++)]. However, the nitrogen and oxygen atoms N1 and O3 possess large negative charges, resulting in the positive charges on the carbon atoms C2, C5, C6 and C12. Moreover, there is no difference in charge distribution observed in all hydrogen atoms except the H22 hydrogen atom (H22= 0.466, 0.464, 0.453 & 0.456 in RHF/6-31, RHF/6-31++, DFT-B3LYP/6-31 and DFT-B3LYP/6-31++ respectively. The large positive charge on H22 is due to the large negative charge accumulated on the N1 atom.

Table 4 Natural atomic charges of efavirenz

Atom	MPA				NPA			
	B3LYP/ 6-31G(d,p)	B3LYP/ 6-31++G(d,p)	RHF/ 6-31G(d,p)	RHF/ 6-31++G(d,p)	B3LYP/ 6-31G(d,p)	B3LYP/ 6-31++G(d,p)	RHF/ 6-31G(d,p)	RHF/ 6-31++G(d,p)
N1	-0.632	-0.432	-0.804	-0.538	-0.698	-0.691	-0.787	-0.778
C2	0.710	0.643	0.983	0.775	0.961	0.947	1.142	1.127
O3	-0.489	-0.172	-0.649	-0.315	-0.560	-0.553	-0.635	-0.632
C4	-0.060	-0.380	0.154	0.318	0.127	0.120	0.184	0.185
C5	0.057	0.045	-0.122	-0.053	-0.101	-0.099	-0.136	-0.134
C6	0.312	0.610	0.356	0.295	0.173	0.166	0.230	0.226
C7	-0.097	-0.601	-0.071	-0.558	-0.217	-0.207	-0.188	-0.176
C8	-0.118	0.068	-0.198	0.152	-0.080	-0.091	-0.088	-0.099
C9	-0.073	-0.162	-0.097	-0.260	-0.227	-0.219	-0.194	-0.184
C10	-0.124	-0.533	-0.180	-0.362	-0.257	-0.249	-0.273	-0.265
O11	-0.387	-0.315	-0.488	-0.413	-0.516	-0.516	-0.619	-0.614
C12	0.868	1.036	1.229	1.218	1.140	1.106	1.305	1.257
F13	-0.267	-0.270	-0.378	-0.384	-0.344	-0.344	-0.403	-0.394
F14	-0.265	-0.282	-0.377	-0.404	-0.346	-0.344	-0.404	-0.395
F15	-0.261	-0.253	-0.385	-0.383	-0.354	-0.351	-0.414	-0.405
C16	0.143	0.063	-0.059	-0.454	-0.110	-0.089	-0.151	-0.161
C17	-0.064	-0.229	-0.080	0.486	0.084	0.077	0.096	0.118
C18	-0.125	0.251	-0.092	-0.180	-0.322	-0.321	-0.307	-0.305
C19	-0.204	-0.582	-0.243	-0.488	-0.474	-0.461	-0.459	-0.439
C20	-0.205	-0.527	-0.242	-0.444	-0.474	-0.462	-0.459	-0.440
Cl21	-0.009	0.271	0.014	0.269	0.017	0.026	-0.002	0.004
H22	0.284	0.370	0.345	0.407	0.453	0.456	0.466	0.464
H23	0.159	0.219	0.252	0.255	0.284	0.283	0.292	0.288
H24	0.111	0.142	0.185	0.165	0.259	0.257	0.257	0.252
H25	0.094	0.107	0.166	0.148	0.246	0.245	0.244	0.240
H26	0.149	0.257	0.192	0.241	0.297	0.293	0.290	0.282
H27	0.117	0.150	0.136	0.116	0.253	0.247	0.243	0.233
H28	0.126	0.175	0.156	0.130	0.266	0.262	0.262	0.254
H29	0.127	0.158	0.147	0.110	0.257	0.252	0.248	0.238
H30	0.124	0.173	0.152	0.148	0.265	0.261	0.260	0.253

4.5 Vibrational analysis

The FTIR and FT-Raman spectra of efavirenz are shown in Figs. 3 and 4. The observed and calculated frequencies using RHF/6-31G(d,p), RHF/6-31++G(d,p), B3LYP/6-31G(d,p), and B3LYP/6-31++G(d,p) methods along with their relative intensities and assignments of efavirenz are summarized in Table 5. The calculated (RHF & B3LYP) vibrational spectra were shown in Fig. 5. Since the calculated vibrational wavenumbers were known to be higher than the experimental ones, they were scaled down by the wavenumber linear scaling procedure of Yoshida et al [16] by using the expression:

$$\nu_{obs} = (1.0087 - 0.0000163\nu_{calc.})\ \nu_{calc.}$$

Comparison of the frequencies calculated at RHF and B3LYP with experimental values (Table 5) reveals the over estimation of the calculated vibrational modes due to neglect of anharmonicity in real system. Inclusion of electron correlation in DFT to a certain extent makes the frequency values smaller in comparison with the RHF frequency data.

In the aromatic ring (R1) C–H stretching vibrations are usually strong in the Raman spectrum. The ν(CH) ring modes are assigned at 3091 and 3027 cm^{-1} [17] in the Raman spectrum. The corresponding calculated values are 3083 and 3053 cm^{-1} and thus coincide well with the experimental observations. Ring

deformations are calculated to be 1504 and 1511 cm^{-1} and are well correlated with observed bands at 1498 cm^{-1} in the Raman spectrum and at 1500 cm^{-1} in the IR spectrum. Out of plane deformations of R1[oop(CH)] are calculated at 981 and 987 cm^{-1} and matches well with IR spectra.

In the oxazine ring (R2) N–H stretching vibration is usually strong in the IR spectrum. The ν(NH) wavenumber in ring is assigned at 3527 cm^{-1} in the IR spectrum. It is calculated to be 3455 cm^{-1}. R2[ν(C=O)] stretch is calculated to be 1794 cm^{-1} and are assigned to the bands at 1750 cm^{-1} in the IR spectrum and at 1749 cm^{-1} in the Raman spectrum. An additional significant feature of efavirenz binding to HIV-1 RT is the presence of a hydrogen bond to the main chain C=O of residue 101, which is not present in the nevirapine complex [18]. Ring deformation (NH) is calculated to be 1450 cm^{-1} and it is observed at 1454 cm^{-1} in the Raman spectrum and at 1430 cm^{-1} in the IR spectrum.

The ν(CH2) stretching vibration of the cyclopropyl ring (R3), whose is assigned to 3324 cm^{-1} in the IR spectra and the calculated value is 3103 cm^{-1} in DFT method. CH2 wagging mode occurs at 1084 cm^{-1} in the IR spectrum. The corresponding DFT calculated values are found to be at 1075 and 1077 cm^{-1}. The rocking modes of CH2 group give rise to the medium intensity bands at 863 cm^{-1} in the Raman spectra. The corresponding DFT calculated wavenumbers are 822 cm^{-1}, as shown in Table 5.

The fluoromethyl group is present in the molecule which is directly connected to the oxazine ring. The symmetric CF3 stretching mode (CF3) appears at a lower energy, in the range 700–800 cm^{-1}, compared to its asymmetric stretching (CF3) which appear in the range 1100–1200 cm^{-1}. The rocking modes of CF3 appear to have variable magnitudes in CF3 containing benzene. The stretching mode ν(C≡C) at the calculated wavenumber 2266 cm^{-1} correspond to the observed bands at 2249 cm^{-1} in the IR spectrum. The vibrational modes calculated to be 865 and 870 cm^{-1} have a major contribution from the internal coordinate corresponding to the deformation of C14C15. Notice that the most evident discrepancies between the experimental and calculated spectra are associated with the stretching modes of the amide synthon, showing its participation in hydrogen bonds. This observation supports the assumption that the amide synthon plays very important role in stabilizing the crystalline structure of efavirenz.

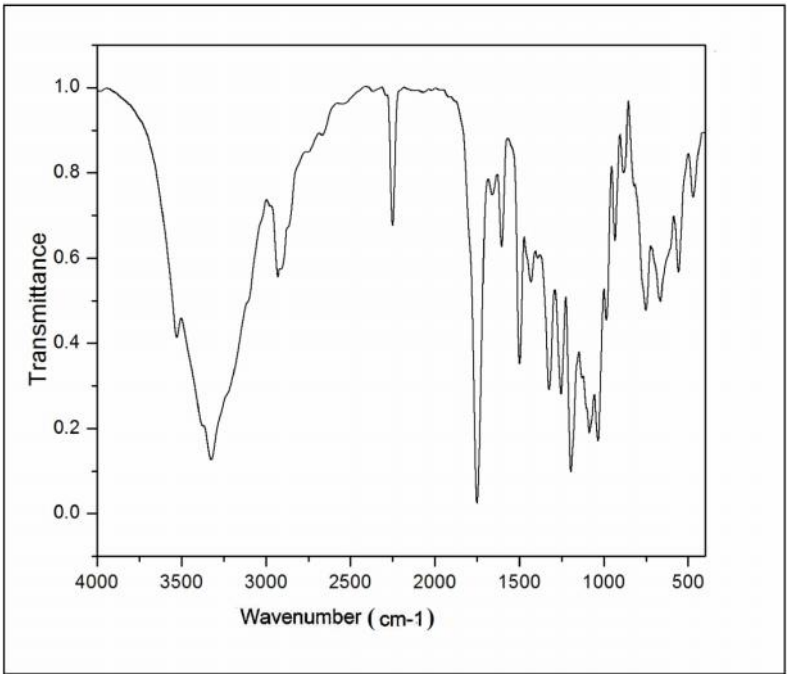

Fig. 3 FTIR spectrum of efavirenz

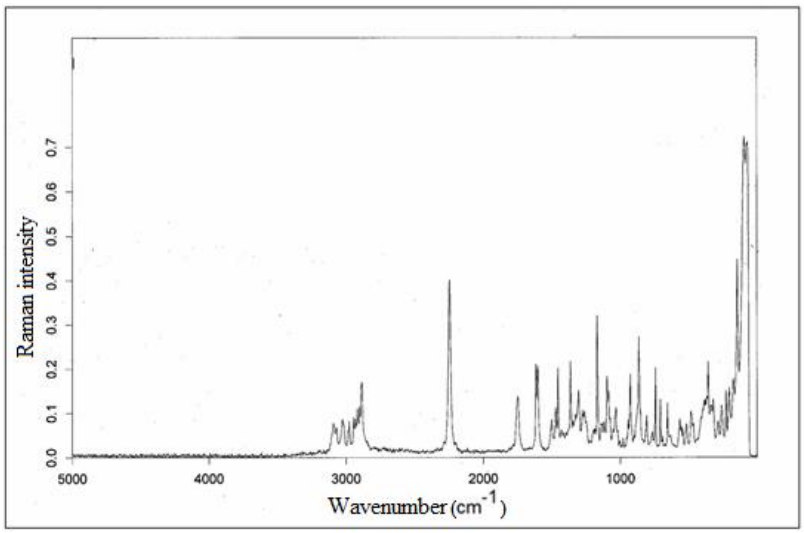

Fig. 4 FT-Raman spectrum of efavirenz

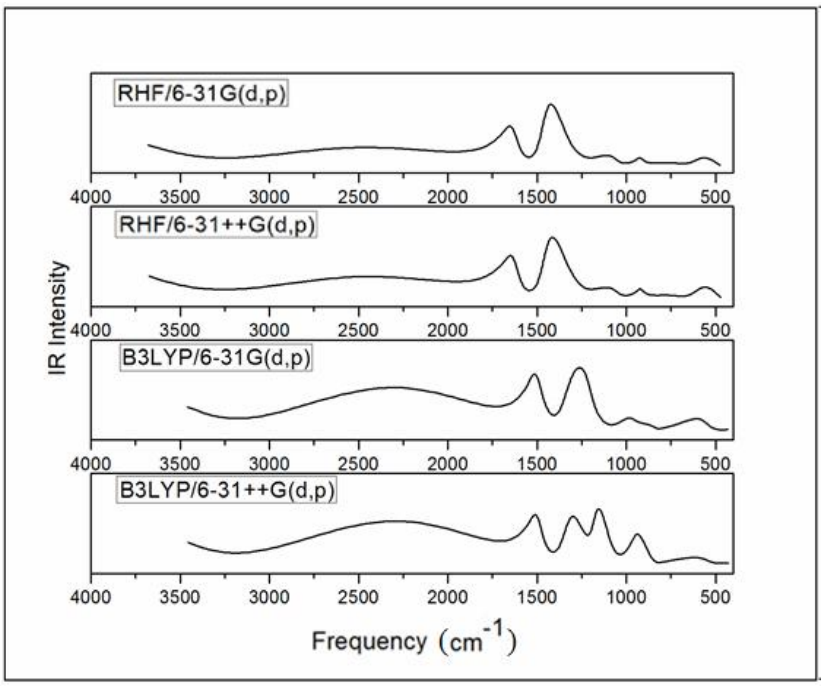

Fig. 5 TheCalculated IR spectrum of efavirenz

Table 5 Selected observed and calculated vibrational assignments of efavirenz

Observed wavenumber (cm^{-1})		Calculated wavenumber (cm^{-1})								Assignment
		RHF/ 6-31 G(d,p)		RHF/ 6-31++ G(d,p)		B3LYP/ 6-31 G(d,p)		B3LYP/ 6-31++ G(d,p)		
FTIR	FT-Raman	Unscal	scaled	Unscal	scaled	Unscal	scaled	Unscal	scaled	
3527		3893	3680	3888	3675	3644	3459	3639	3455	R2[ν(NH)]
3324		3401	3242	3399	3240	3251	3107	3247	3103	R3[ν(CH2)]
		3390	3232	3389	3231	3238	3095	3233	3091	R3[ν(CH2)]
	3091	3387	3229	3385	3228	3225	3084	3224	3083	R1[ν(CH)]
	3027	3358	3203	3357	3203	3192	3054	3191	3053	R1[ν(CH)]
		3331	3179	3333	3181	3159	3024	3160	3025	R3[ν(CH2)]
		3308	3158	3306	3157	3155	3020	3151	3017	R3[ν(CH2)]
2930		3301	3152	3299	3150	3152	3017	3148	3014	R3[ν(CH2)]
2249		2555	2471	2540	2457	2349	2279	2335	2266	ν(C≡C)
1750	1749	2044	1994	2010	1962	1872	1831	1833	1794	R2[ν(C=O)]
1498	1500	1674	1643	1668	1637	1536	1511	1529	1504	R1[δ(CH2)]+R2[ν_{ring}]
		1633	1604	1630	1601	1494	1471	1493	1470	R1[s(CH2)]
1430	1454	1599	1571	1596	1568	1480	1457	1473	1450	R2[δ(NH)+ ν_{ring}(NC)]]+ R1[δ(CH)]
1323	1363	1518	1494	1512	1488	1401	1381	1395	1375	R3[oop(CH)]
1194	1169	1289	1273	1285	1269	1207	1194	1186	1173	R1[δ(CH)]
		1268	1253	1264	1249	1192	1179	1173	1161	ν(CF3)
		1238	1224	1235	1221	1160	1148	1157	1145	ν(CF3)
	1097	1227	1213	1223	1209	1115	1104	1111	1101	R3(ν_{ring})
1084		1207	1194	1205	1192	1087	1077	1085	1075	R3[ω(CH2)]+R3[δ(CC 19H)]
984		1095	1085	1092	1082	994	987	988	981	R1(oop(CH)
932	927	1044	1035	1038	1029	946	940	945	939	R3[ν_{ring}]+oop(C14C20 H)
881		1021	1013	1015	1007	918	912	908	902	R1(oop(CH))
	863	951	945	948	942	875	870	870	865	oop(C14C15)
		903	898	899	894	826	822	826	822	R3(ν_{ring})
		897	892	894	889	825	821	823	819	R3(ν_{ring})
750	742	843	839	839	835	749	746	746	743	R2[oop(CO)]
	706	787	784	784	781	718	716	713	711	δ(CF3)+ν(CF3)

ν- stretching, δ - deformation, oop - out of plane, ω- wagging, ρ-rocking, s-scissoring

Table 6 The calculated thermodynamic parameters of efavirenz

Parameter	RHF/ 6-31G(d,p)	RHF/ 6-31++G(d,p)	B3LYP/ 6-31G(d,p)	B3LYP/ 6-31++G(d,p)
Total Energy(a.u)	-1497.11	-1497.14	-1503.56	-1503.61
Zero point energy(kcal/mol)	140.085	139.595	129.528	128.929
Rotational Constants(GHz)	0.347	0.345	0.341	0.338
	0.197	0.197	0.194	0.194
	0.184	0.184	0.182	0.182
Entropy				
Total	118.745	119.178	145.985	144.177
Translational	43.139	43.139	43.139	43.139
Rotational	34.501	34.508	34.543	34.555
Vibrational	61.376	61.783	68.303	66.484
Dipole moment(Debye)	4.6930	4.9634	4.3503	5.0071

4.6 Thermodynamic properties

Several calculated thermodynamic parameters are presented in Table 6. Scale factors have been recommended [19] for an accurate prediction in determining the zero-point vibrational energies and the entropy S. The variation in the ZPVEs seems to be insignificant. The total energies found to decrease with increase of the basis sets dimension. The changes in the total entropy of efavirenz at room temperature at different basis sets are only marginal.

5. Conclusion

The geometry of efavirenz was optimized with RHF and DFT-B3LYP methods using 6-31G(d,p) and 6-31++G(d,p) basis sets. The complete molecular structural parameters and thermodynamic properties of the optimized geometry of the compound have been obtained from ab initio and DFT calculations. The bond order and atomic charges of the title molecule have been studied by both RHF and DFT methods. The vibrational frequencies of the compound have been precisely assigned and analyzed and the theoretical results were compared with the experimental vibrations. The energies of important MO's, absorption wavelength (λ_{max}), oscillator strength and excitation energies of the compound were also determined from TD-DFT method and compared with the experimental values. Thus the present investigation provides the complete vibrational assignments, structural information and electronic properties of the compound which may be useful to upgrade the knowledge on efavirenz.

References

1. J.C. Adkins, S. Noble, Drugs, 1998, 56,1055.
2. Du Pont Pharmaceuticals Company, Sustiva (efavirenz capsules), prescribing information, 17 Sept.,1998; http: /www.sustiva.com
3. L. Bacheler, O. Weislow, S. Snyder, G. Hanna, in: 12thWorld AIDS Conference, Geneva, 1998, Abstract 41213.
4. D. Mayers, J. Jemsek, E. Eyster, K. Tashima, M. Thompson, N. Ruiz, in: 12th World AIDS Conference, Geneva, 1998, Abstract 22340.
5. S. Riddler, J. Kahn, C. Hicks, D. Stein, J. Horton, N. Ruiz, in: 12th World AIDS Conference, Geneva, 1998, Abstract 12359.
6. D. Havlir, C. Hicks, J. Kahn, S. Riddler, Q. Lino, N. Ruiz, in: 38th Interscience Conference on Antimicrobal Agents and Chemotherapy, San Diego, CA, 1998, Abstract I-104.
7. M.J. Frisch, G.W. Schlegel, H.B. Scuseria, G.E. Scuseria, M.A. Robb, J.R. Cheeseman, J.A. Montgomery, T. Vreven, K.N. Kudin, J.C. Burant, J.M. Millam, S.S. Iyengar, J. Tomasi, V. Barone, B. Mennucci, M. Cossi, G. Scalmani, N. Rega, G.A. Petersson, H. Nakatsuji, M. Hada, M. Ehara, K. Toyota, R. Fukuda, J. Hasegawa, M. Ishida, Nakajima, Y. Honda, O. Kitao, H. Nakai, M. Klene, X. Li, J.E. Knox, H.P. Hratchian, J.B. Cross, C. Adamo, J. Jaramillo, R. Gomperts, R.E. Stratmann, O. Yazyev, A.J. Austin, R. Cammi, C. Pomelli, J.W. Ochterski, P.Y. Ayala, K. Morokuma, G.A. Voth, P. Salvadorm, J.J. Dannenberg, V.G. Zakrzewski, S. Dapprich, A.D. Daniels, M.C. Strain, O. Farkas, D.K. Malick, A.D. Rabuck, K. Raghavachari, J.B. Foresman, J.V. Ortiz, Q. Cui, A.G. Baboul, S. Clifford, J. Cioslowski, B.B. Stefanov, G. Liu, A. Liashenko, P. Piskorz, I. Komaromi, R.L. Martin, D.J. Fox, T. Keith, M.A. Al-Laham, C.Y. Peng, A. Nanayakkara, M. Challacombe, P.M.W. Gill, B. Johnson, W. Chen, M.W. Wong, C. Gonzalez, J.A. Pople, Gaussian 03, Revision C. 02, Gaussian, Inc.,Wallingford, CT 06492, 2003.
8. H.B. Schlegel, J. Comput. Chem., 1982, 3, 214.
9. A.D. Becke, Phys. Rev. A, 1988, 38, 3098.
10. C. Lee, W. Yang, R.G. Parr, Phys. Rev. B, 1988, 37, 785.
11. B.G. Johnson, M.J. Frisch, Chem. Phys. Lett.,1993, 216, 133.
12. W.J. Hehre, L. Radom, P.V.R. Schleyer, A.J. Pople, Ab initio Molecular Orbital Theory, Wiley, New York, 1989.
13. Z. Dega-Szafran, A. Katrusiak, M. Szafran, J.Mol. Struct.,2005, 741, 1.
14. L.E. Sutton, Tables of interatomic distances and configuration in molecules and ions, Chemical society, Burlington House,W.I, 18,1958.

15. R.M. Silverstein, G.C. Bassler, T.C. Morrill, Spectrometric Identification of Organic Compounds, 5th ed., John Wiley & Sons, Inc., New York,1981.
16. H. Yoshida, K. Takeda, J. Okamura, A. Ehara, H. Matsurra, J. Phys. Chem. A. 106 (2002) 3586.
17. S. Mishra, P. Tandon, A.P. Ayala, Study on the structure and vibrational spectra of efavirenz conformers using DFT:Comparison to experimental data, SpectrochimicaActa Part A, 2012, 88, 116.
18. J. Lindberg, S. Sigurdsson, S. Lowgren, H.O. Andersson, C. Sahlberg, R. Noreen, K. Fridborg, H. Zhang, T. Unge, Eur, J. Biochem. 2002, 269 (6), 1670.
19. M. AlcoleaPalafox, Int. J. Quantum. Chem. 2001, 77, 661.

*****